ACS NANO

www.acsnano.org

ARTICLE

Dual Type-II Colloidal Quantum Wells for Efficient Nonlinear Optical Limiting

Junhong Yu,*,# Emek Goksu Durmusoglu,# Yunfei Ren, Wenhui Fang, Yubu Zhou, Linghao Chu, Baiquan Liu,* and Hilmi Volkan Demir*

Cite This: *ACS Nano* 2025, 19, 9273−9281

Read Online

ACCESS | Metrics & More | Article Recommendations | Supporting Information

ABSTRACT: **Colloidal II−VI nanocrystals have garnered significant research attention in nonlinear optical applications due to their low-cost synthesis, photophysical tunability, and ease of device integration. Herein, we report that dual-type II CdSe/CdTe/CdSe colloidal quantum wells (CQWs) with core/crown/crown structures achieve remarkable nonlinear optical limiting capabilities driven by an exceptionally large nonlinear absorption coefficient. Open aperture *Z*-scan reveals that these dual-type II CQWs exhibit a third-order nonlinear absorption coefficient of 33.1 cm/GW and an ultralow optical limiting threshold (0.71 GW/cm^2), which is superior to that of any other reported colloidal semiconductor nanocrystals while also being comparable to existing two-dimensional (2D) dichalcogenide sheets. Photophysical analysis indicates that such a remarkable nonlinear optical performance in dual-type II CQWs can be primarily ascribed to the efficient excited state absorption (i.e., the sequential two-photon absorption), which benefits from the ultrafast and uniform formation of charge separation states in the dual type-II heterostructures.**

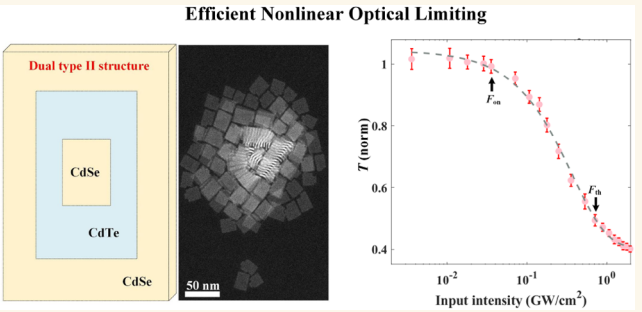

KEYWORDS: *optical limiting, colloidal quantum wells, CdSe nanocrystals, optical nonlinearity, type II*

INTRODUCTION

Third-order nonlinear optical (NLO) materials are fundamental to advancements in optoelectronics for optical power limiting (OL),[1−4] nonlinear optical amplification,[5,6] and infrared biolabeling.[7,8] Specifically, OL indicates the capability of an NLO material to attenuate the transmission of intense light,[9] these are essential for safeguarding fragile instruments and human eyes from damage caused by lasers. In recent decades, many efforts have been devoted to various types of organic (e.g., phthalocyanines,[10] porphyrins[11]), inorganic (e.g., carbon derivatives,[12] metal oxides,[13] metal dichalcogenides semiconductors[14]), and inorganic−organic (e.g., metal−organic frameworks,[15] hybrid halide perovskites[16]) materials to promote the OL performance. Besides the above-mentioned materials, colloidal semiconductor nanocrystals are also good candidates considering the combination of quantum-confinement enhanced optical nonlinearity[17] with their intrinsic advantages (i.e., low-cost synthesis, photophysical tunability, and ease of device integration).[18−23] However, constrained by relatively low cross sections of two-photon absorption (TPA), efficient linear carrier recombination, and ultrafast Auger effects, II−VI colloidal quantum dots (CQDs) or nanorods (CNRs) only exhibit poor OL responses (e. g., the third-order nonlinear absorption coefficient of ∼1 cm/GW and an OL threshold up to 100 GW/cm^2).[24−27]

A viable strategy to improve the third-order optical nonlinearity of colloidal semiconductor nanocrystals lies in the formation of type-II heterostructured colloidal quantum wells (CQWs) due to their unique properties: (i) both the local field effect (i.e., the geometrical contribution) and the electronic confinement (i.e., the electronic contribution) favor the anisotropic two-dimensional (2D)-shape of nanoplatelets, resulting in an improved TPA cross-section compared to CQDs and CNRs with similar volumes;[28,29] (ii) the spatially separated electrons and holes in the type-II CQWs allows a linear carrier recombination extended lifetime to hundreds nanoseconds,[30,31] which increases the probabilities of the sequential TPA (i.e., excited state absorptions) in the third-order nonlinear process; and (iii) the heterobarrier with a

Received: January 7, 2025
Revised: February 25, 2025
Accepted: February 25, 2025
Published: March 2, 2025

https://doi.org/10.1021/acsnano.5c00391
ACS Nano 2025, 19, 9273−9281

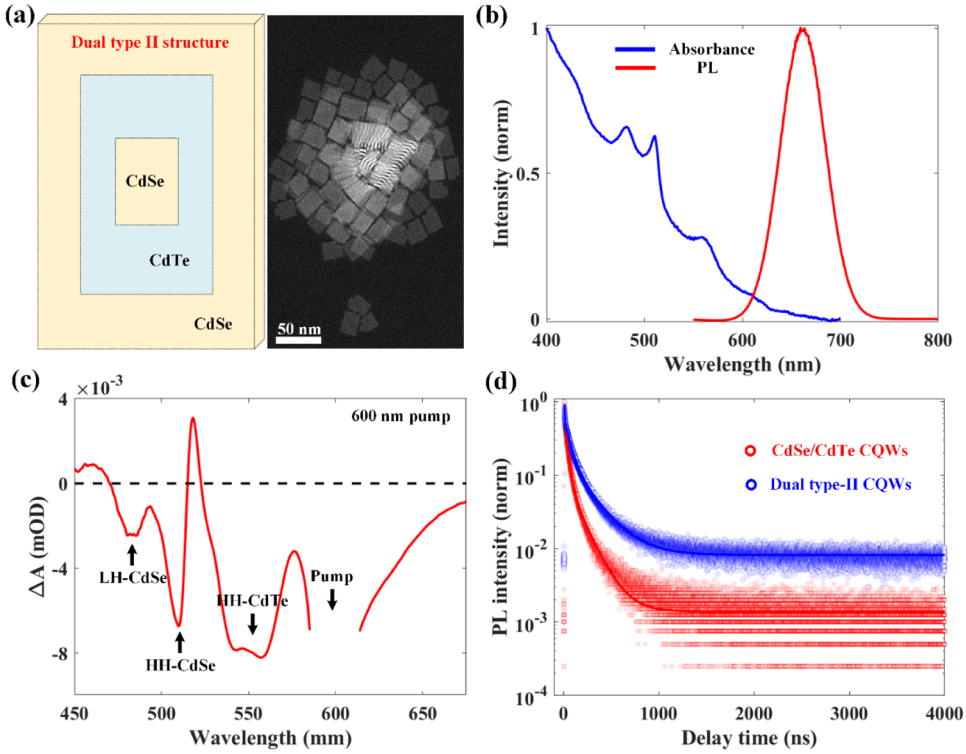

Figure 1. Optical and structure properties of dual type-II CQWs. (a) The core/crown/crown structure (left panel) and the representative HAADF-STEM image (right panel). (b) Normalized photoluminescence (red line) and absorption (blue line) spectra. For photoluminescence, excitation is at 400 nm. (c) TA spectra at a probe delay of 1.5 ps of dual type-II CQWs pumped with a 600 nm pulse. The excitation fluence is about 10 μJ/cm^2. (d) TRPL of CdSe/CdTe CQWs (red dots) and dual type-II CQWs. (blue dots) with exponential fittings (solid lines).

complicated energy conservation requirement and reduced carrier wave function overlap in the type-II CQWs renders the Auger process inefficient compared to the type-I CQWs.[32,33] Recently, our group[34,35] and Ithurria et al.[36,37] reported the successful synthesis and emission applications of multicrowned CdSe/CdTe/CdSe CQWs with the advantage of dual type-II transition channels. These novel CQWs not only possess the necessary criteria discussed above but may also present unique advantages to open exciting new prospects for OL applications.

In this work, we have revealed that CdSe/CdTe/CdSe multicrowned CQWs exhibit strong reverse saturation absorption (RSA) responses driven by a giant third-order nonlinear absorption coefficient up to ~33.1 cm/GW under nanosecond laser pulse excitations, making them excellent candidates for OL applications. The OL performance test demonstrates that these dual type-II CQWs possess an onset excitation density of ~0.04 GW/cm^2 and a limiting threshold value of ~0.71GW/cm^2, which signifies an improvement of more than 1 order of magnitude compared to the previous best results in colloidal nanocrystals. We have validated the underlying mechanism responsible for this outstanding OL performance with the unique dual type-II band alignment by analyzing the contributions of genuine TPA and sequential TPA in the third-order optical nonlinear process. Compared with typical CdSe/CdTe CQWs, these dual type-II CQWs exhibit a density of type-II charge-transfer states approximately five times larger, more uniform separation of both carriers, and less band bending at the interface, these greatly enhance their third-order nonlinear absorption coefficient with higher probabilities of excited-state absorption.

RESULTS

The multicrowned CdSe/CdTe/CdSe CQWs investigated in this work are synthesized by using the 4 monolayers (ML) core CdSe CQWs (i.e., consisting of 5 Cd layers and 4 Se layers, arranged such that each pair of Cd layers sandwiches one Se layer) as a seed, enabling a one-pot growth process for the inner CdTe crown and outer CdSe crown layers (see Methods Section for details). The crown layer describes a lateral expansion of the core CQW that enhances the optical properties and absorption cross-section of as-synthesized core CQW. As schematically shown in the left panel of Figure 1a, this multicrowned CQW architecture supports two different type-II transitions: one from the CdSe core to the CdTe crown and another from the CdTe crown to the CdSe crown, which benefits the third-order nonlinear optical process and will be discussed later. The high-angle annular dark-field scanning transmission electron microscopy (HAADF-STEM) image of dual type-II CQWs is presented in Figure 1a, which indicates that, after the growth of two crowns, the lateral extent is uniform and the lateral size reaches 23.9 nm by 29.6 nm on average. The steady-state optical spectra of dual type-II CQWs are shown in Figure 1b. The absorbance of these dual type-II CQWs exhibits three distinct excitonic peaks, corresponding to the electron/heavy-hole (HH) transition of CdSe at 512 nm, the electron/light-hole (LH) transition of CdSe at 480 nm, and the electron/HH transition of CdTe at 570 nm, consistent with the confinement nature of 4 ML CQWs in the vertical direction.[32,33]

The featureless absorption band observed from 600 to 700 nm, absent in CdSe or CdTe CQWs, is ascribed to the transition of charge transfer (CT) states and accounts for the

https://doi.org/10.1021/acsnano.5c00391
ACS Nano 2025, 19, 9273−9281

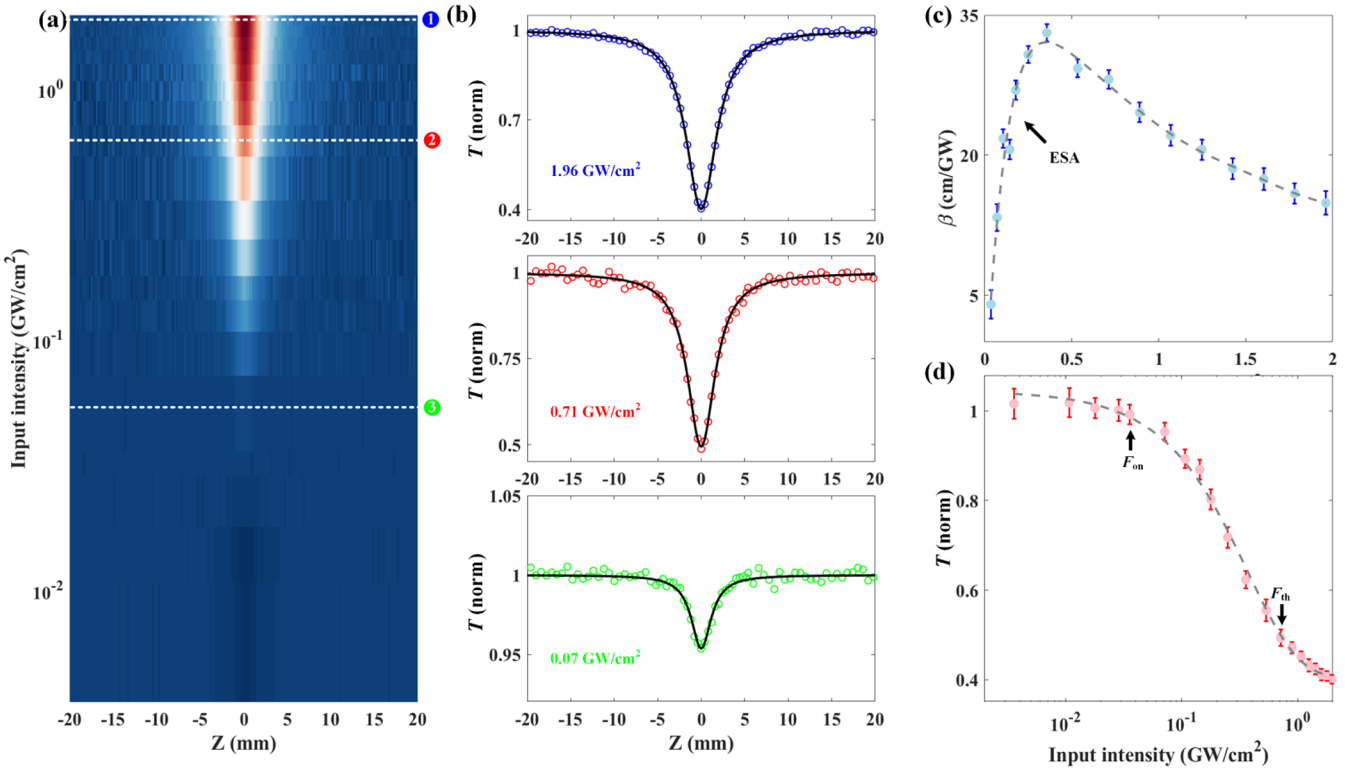

Figure 2. OA *Z*-scan measurements of dual type-II CQWs with different excitation densities. The measured optical transmittance is normalized based on the value when the sample is far away from the focal point. (a) Two-dimensional contour map of 532 nm laser pulse transmittance. *X*-axis: the scan distance. *Y*-axis: the excitation density. (b) Three representative transmittance curves (dots) fitted with the nonlinear transmission equation (black lines). (c) Excitation density-dependent third-order nonlinear absorption coefficient (β). (d) Excitation density-dependence of the normalized transmittance at the focal point ($Z = 0$).

Stokes-shifted broad emission at 645 nm.[38,39] We have also conducted the transient absorption (TA) measurement under 600 nm excitation (i.e., selectively pumped CT states). As shown in Figure 1c, using excitation energies below the bandgap of the core and crowns, photobleaching (PB) of LH-CdSe, HH-CdSe, and HH-CdTe can be well-resolved and emerge instantaneously with a temporal resolution limited rise time of ∼100 fs (see the pulse width of the fs pumping laser in Figure S1), indicating direct carrier generations[38,39,43] and validating the assignment of CT states. More importantly, these CT states with spatially indirect recombination of carriers across the interface (i.e., holes in the CdTe domain and electrons in CdSe domains) could significantly prolong the linear carrier recombination lifetime and thus, boost the probabilities of the sequential TPA (i.e., excited state absorptions) in the third-order nonlinear process. Time-resolved PL (TRPL) measurements shown in Figure 1d reveal a radiative lifetime of ∼73.3 ns for dual type-II CQWs, which is more than one magnitude longer than single component or type I heterostructured colloidal nanocrystals.[40−42] It should be noted that the PL lifetime of typical CdSe/CdTe CQWs (∼46.2 ns) is much shorter compared to the dual type-II sample, implying their different carrier properties and distinct OL performances.

Following the standard test procedure for OL performance,[44] open-aperture (OA) *Z*-scan transmission measurements of the dual type-II CQW solution are carried out with the 532 nm nanosecond pulse excitation (see experimental details in Methods Section). Please note that we calibrate our *Z*-scan system using liquid carbon disulfide as the reference[45] and no clear *Z*-scan curves are recorded with the pure solvent (hexane). The two-dimensional contour map of the transmission curves depending on the on-axis scanning distance (the focal point defined as $Z = 0$) and the input intensity (ranging from ∼0.03 to ∼1.96 GW/cm^2) is shown in Figure 2a, which shows a reduction in transmittance as the focus is approached, indicating the occurrence of reverse saturable absorption (RSA). It is worth mentioning that when the input intensity is low enough (e.g., ∼MW/cm^2), saturable absorption (SA) due to the Pauli blocking has also been identified in dual type-II CQWs (see Figure S2 for details). Assuming a Gaussian intensity distribution for the laser beam, the normalized OA *Z*-scan transmittance is given by the following equation[16,46,47]

$$T(z) = \left[1 + (n-1)\beta L_{\text{eff}}\left(\frac{I_0}{1+(z/z_0)^2}\right)^{n-1}\right]^{-1/(n-1)}, \quad L_{\text{eff}} = \frac{1-e^{-\alpha L}}{\alpha} \tag{1}$$

where I_0 represents the input laser intensity at $Z = 0$, n is the number of absorbed photons in the nonlinear process, Z_0 is the Rayleigh length of the laser beam, L is the sample length, α denotes the linear absorption coefficient, and β is the effective multiphoton absorption coefficient.

The solid black curves in Figure 2b represent the theoretical fits obtained using eq 1 with $n = 2$ (i.e., two-photon absorption, TPA) for three representative input intensities (see the fitting for other input intensities in Figure S3), which show good agreement with the experimental results. The relationship

https://doi.org/10.1021/acsnano.5c00391
ACS Nano 2025, 19, 9273−9281

between the determined parameter β (i.e., TPA coefficients) and the input intensities is shown in Figure 2c, which shows an initial increasing trend followed by a decreasing trend. If only the genuine TPA process (i.e., two photons are concurrently absorbed via an intermediate virtual energy state) is considered, β will decline monotonically with higher input intensities due to a greater depletion of the carrier populations in the ground state.[3,9,14,17,29] Consequently, such a unique behavior of β in dual type-II CQWs implies an indispensable contribution to the sequential TPA process (i.e., the so-called excited state absorption (ESA)), in which the accumulation of carriers at the excited state with increasing input intensities could enhance the third-order nonlinear optical absorption. Meanwhile, as shown in Figure 2d, the OL performance of dual type-II CQWs has been evaluated when the transmittance begins to drop (i.e., the limiting onset, F_{on}) and decreases to half of its linear value (i.e., the limiting threshold, F_{th}). For a quantitative comparison, Table 1 lists the values of β, F_{on}, and

Table 1. Comparison of β and OL Performances (i.e., the Onset and Threshold Input Densities) in Different Materials

	β (cm/GW)	F_{on} (GW/cm^2)	F_{th} (GW/cm^2)
dual type-II CQWs (this work)	33.1	0.036	0.71
CdSe CQDs/CQWs[24−25,26,28,29]	0.07−0.26		
type I CQDs/CQWs[47,48]	0.46−1.48	10.45	82.3
type II CQDs/CQWs[30,49,50]	0.83−3.77	1.48	5.25
lead halide perovskite CNCs[6,16,51]	0.45−35	0.04−0.78	0.68−20.34
TMDC[46,52]	1.69−120	0.004−0.25	0.07−4.53

F_{th} in different types of low-dimensional nanomaterials at similar excitation conditions. It can be seen that dual type-II CQWs show an improvement of more than 1 order of magnitude in third-order optical nonlinearity compared to typical CdSe/CdTe CQWs (see the OA *Z*-scan analysis and OL performances in Figure S4) and other colloidal nanocrystals,[24−26,28−30,49,50] which also becomes comparable to the performance of state-of-the-art perovskite nanocrystals[6,16,51] and two-dimensional transition metal dichalcogenides.[46,52]

In order to understand the origin of such a superior third-order optical nonlinearity, we have first investigated the contribution of the genuine TPA process by exciting CdSe/CdTe/CdSe CQWs at 800 nm. As shown in Figure 3a, these dual type-II CQWs exhibit red emission with an 800 nm laser excitation, which implies the observation of genuine two-photon excited emission considering the absence of energy levels close to the excitation wavelength.[53] It should be noted that unlike other emission species with charge transfers,[54,55] the similarity between the two-photon and one-photon excited PL spectra in dual type-II CQWs suggests that the photo-excited carriers in both cases relax to the same lowest energy level (i.e., the CT state), indicating an efficient and uniform charge separation. The genuine two-photon excited emission is further confirmed via the log−log plot of the emission integral as a function of the excitation fluences (see the bottom panel of Figure 3a), where the nearly quadratic dependence rules out the Auger-type PL upconversion.[4] Therefore, the genuine TPA coefficient (β) can be quantitatively evaluated based on OA Z-scan measurements excited at 800 nm.

The top panel of Figure 3b shows the OA *Z*-scan curves of hexane as a reference and the CQWs solution with the excitation intensity of 1.96 GW/cm^2. The horizontal *Z*-scan curve of the hexane suggests that the solvent's nonlinear absorption is minimal. To further prove that the *Z*-scan response with 800 nm excitation comes from the genuine TPA process, we plotted $\ln(1-T_z)$ versus $\ln(I_z)$ (see the bottom panel of Figure 3b), where a slope of 1 is consistent with the model proposed in ref 56. (i.e., the slope for three-photon absorption will be 2). Similar to the analysis in Figure 2, we have collected the OA *Z*-scan data with 800 nm excitation as a function of input intensities (see the pseudocolor plot in the top panel of Figure 3c and the individual *Z*-scan curves in Figure S5). Through the analysis of each nonlinear absorption response curve using eq 1 with $n = 2$, we have determined the genuine TPA coefficients and the corresponding OL performance of dual type-II CQWs. As shown in the bottom panel of Figure 3c, the genuine TPA coefficient of dual type-II CQWs is only ∼1 cm/GW, which slightly exceeds or is comparable to those of previously studied colloidal nanocrystals.[24−30,47−50] Such a genuine TPA coefficient only causes a 5% transmittance reduction with an input intensity of 1.96 GW/cm^2 (see the transmittance analysis at $Z = 0$ in Figure S6). As a result, it is plausibly attributed to the remarkable OL performance of dual type-II CQWs due to the sequential TPA process (i.e., excited-state absorption with long-lived excited states).

Next, we investigated the photophysics of excited-state carriers in dual type-II CQWs by performing femtosecond transient absorption (TA) measurements excited at 400 nm (see experimental details in Methods Section). Please note that to suppress the impact of multiexciton effects, a weak excitation fluence of ∼20 μJ/cm^2 is adopted, which corresponds to generating approximately 0.3 electron−hole pairs.[28,31,39] Here to confirm the advantage of dual type-II CQWs, TA results of typical type-II (CdSe/CdTe CQWs) are also presented for comparison. As shown in Figure 4a,b, negative photobleaching (PB) features of HH-CdSe, HH-CdTe, and CT arising from the Pauli blocking are identified for both kinds of CQWs with peak positions matching well with the steady-state absorption spectra (see Figure 1b). More importantly, CdSe/CdTe/CdSe CQWs with the dual type-II transitions expectedly exhibit a much stronger TA signal from CT transitions compared to CdSe/CdTe CQWs. Based on the normalized PB intensity integral of the CT band in the TA spectra,[43] we can roughly estimate that the ratio of CT state density in these two CQWs is about 5:1. Moreover, it can be seen that the amplitudes of the TA signal from the CdSe domains are almost identical for these two CQW heterostructures, while the PB band of HH-CdTe in dual type-II CQWs becomes shallower and broader compared to that in CdSe/CdTe CQWs. This observation is consistent with recent wave function distribution calculations,[34,35] which indicate that the hole wave function in dual type-II CQWs is less accumulated at the interface and more uniformly distributed throughout the CdTe domain.

In addition to the difference in transient spectra difference, dual type-II CQWs also exhibit unique carrier separation kinetics. As shown in Figure 4c, the PB bands of HH-CdSe and HH-CdTe for both CQWs show a rapid rise (0.25 ± 0.03 ps), which further validates the direct carrier generation under 400 nm excitation. Note that a rise time longer than the pulse

https://doi.org/10.1021/acsnano.5c00391
ACS Nano 2025, 19, 9273−9281

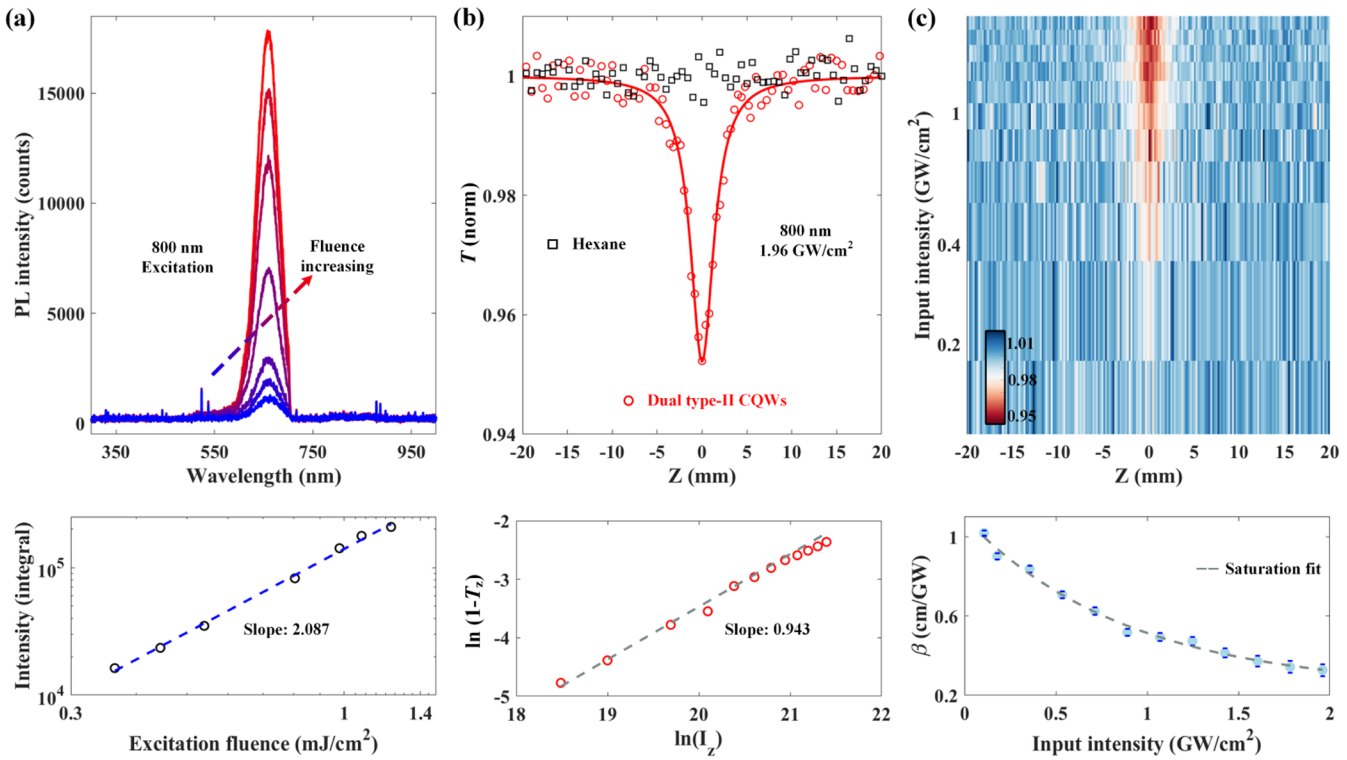

Figure 3. Characterizations of the genuine TPA process in dual type-II CQWs. (a) Top: Excitation fluence-dependent PL spectra of dual type-II CQWs with an 800 nm excitation. Bottom: The log−log fitting of the excitation fluence-dependent emission integral intensity with a slope of ~2.1. (b) Top: OA *Z*-scan curves of dual type-II CQWs (red), and hexane (black) with an 800 nm excitation. The excitation intensity is ~1.96 GW/cm^2. The solid lines correspond to the theoretical fits derived from the *Z*-scan analysis. Bottom: The plot of ln $(1-T_z)$ versus ln (I_z) at various input intensities. A linear fitting using the genuine TPA model is shown as the dashed line. (c) Top: two-dimensional contour map of 800 nm laser pulse transmittance. *X*-axis: the scan distance. *Y*-axis: the excitation density. Bottom: The genuine TPA coefficient (β) versus the input density.

width can be ascribed to the hot carrier cooling process.[43,57,58] For CdSe/CdTe CQWs, the formation of the slow PB band for CT (0.62 ± 0.05 ps) closely matches the fast decay process of CdTe-HH PB (0.63 ± 0.05 ps), aligning with electron transfer from the CdTe crown to the interface. There is also a long lifetime component in PB kinetics, due to the state filling of carriers.[38,39] It is worth mentioning that the PB band of CdSe-HH does not show a noticeable fast decay process, indicating a minimal hole transfer process from the CdSe core to the interface (i.e., an inefficient carrier separation process).[43] In contrast, for dual type-II CQWs, the more rapid decay process of CdSe-HH PB (0.41 ± 0.04 ps) and CdTe-HH PB (0.52 ± 0.04 ps) both contribute to the PB band formation process of CT states (i.e., two rising lifetime components of 0.38 ± 0.04 ps and 0.47 ± 0.04 ps are resolved), suggesting that holes and electrons are transferred and separated in a faster, more efficient, and uniform manner.

The uniform distributions of carriers in dual type-II CQWs can be further validated by the transient peak energy shifting of the CT bands. In typical type-II heterostructures, the creation and decay of the transient electric field cause a blueshift−redshift crossover due to band bending[31] (see the schematic illustrations in Figure S7). Please note that the time-independent peak positions of single domain-related transition features are understandable in type-II CdSe/CdTe CQWs since the quickly spatially localized photoexcited carriers hinder the formation of single domain multiexcitons and the transient electric field accumulated at the domain interface will mainly affect the interdomain transitions (i.e., CT bleaching band). As shown in Figure 4d, the peak energy diffusion for a CT transition crossover in CdSe/CdTe/CdSe CQWs has been largely suppressed, and more importantly, such a CT energy shift is almost independent of increased excitation fluences (see the fluence-dependent TA results and CT energy shifts in Figures S8 and S9), violating the linearly increasing trend with the cube-root fluence in CdSe/CdTe CQWs. Therefore, as illustrated schematically in Figure 4e, in comparison to the conventional CdSe/CdTe type-II CQWs, we can briefly conclude that CdSe/CdTe/CdSe CQWs with the dual type-II band alignments not only support an increased density of CT states (i.e., 5-fold enhancement) but also induce an efficient charge transfer process (i.e., both carriers are transferred with faster kinetics) and fewer carrier accumulation at the interface (i.e., the suppressed band bending effect), resulting in a prolonged lifetime of the excited carriers (see the comparison of CT PB dynamics in Figure S10 and TRPL in Figure 1d) and suppressed Auger recombination, which enhances the sequential TPA contributions to the third-order optical nonlinear process.

CONCLUSIONS

In summary, the third-order nonlinear optical response of CdSe/CdTe/CdSe CQWs has been systematically investigated. Open aperture *Z*-scan measurements reveal that these dual type-II CQWs have a strong RSA response with optimized optical limiting performance. The optical limiting threshold of 0.71 GW/cm^2 with a third-order nonlinear absorption coefficient up to 33.1 cm/GW is vastly higher than those of

https://doi.org/10.1021/acsnano.5c00391
ACS Nano 2025, 19, 9273−9281

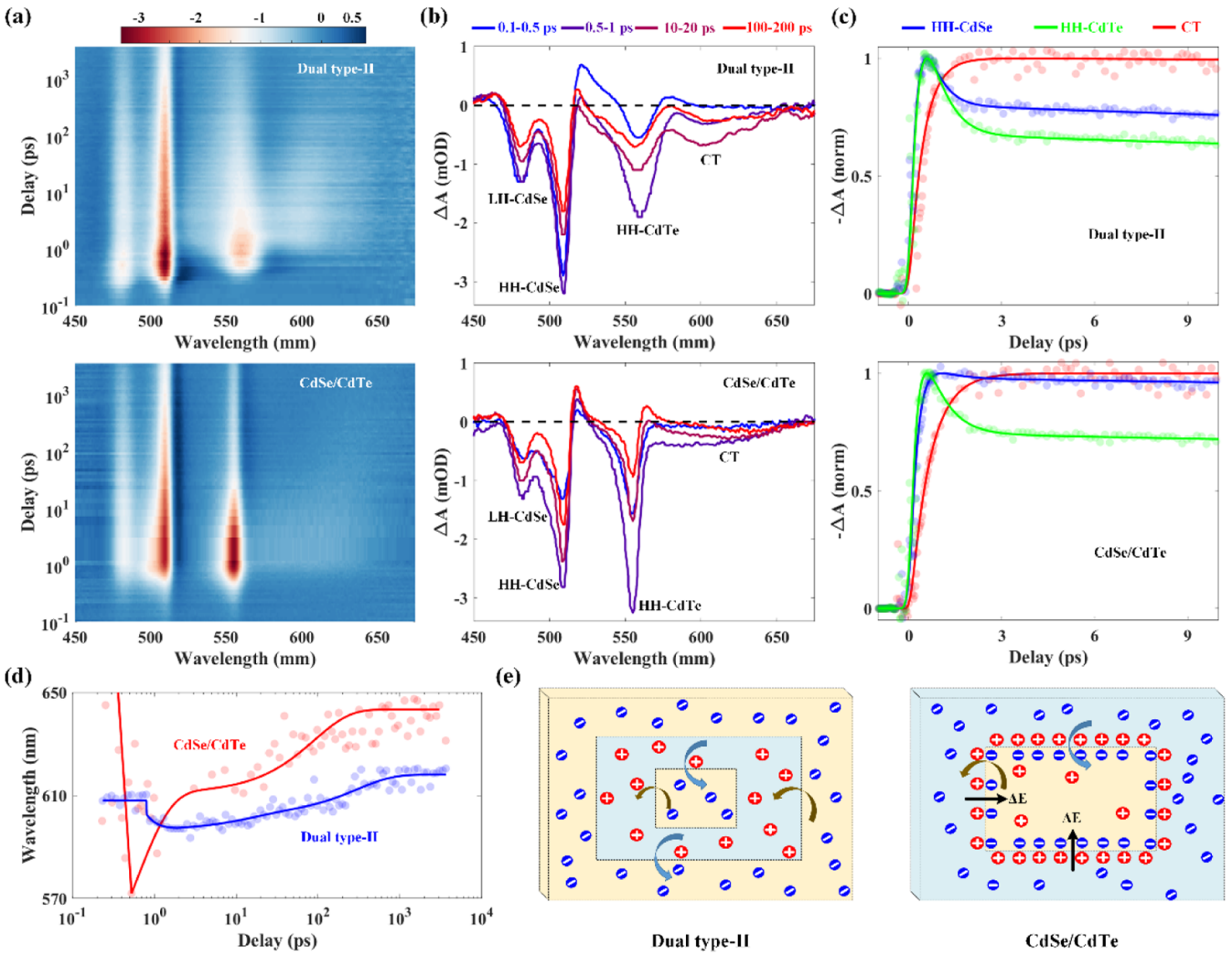

Figure 4. Characterizations of the sequential TPA process in dual type-II CQWs. (a) Top: Pseudocolor TA map of dual type-II CQWs. Bottom: Pseudocolor TA map of CdSe/CdTe CQWs. The pump wavelength is 400 nm and the pump fluence is 20.4 μJ/cm^2. (b) Top: TA spectra of dual type-II CQWs at different delay times. Bottom: TA spectra of dual type-II CQWs with different delays. (c) Top: Bleaching kinetics of HH-CdSe, HH-CdTe, and CT in dual type-II CQWs. Bottom: Bleaching kinetics of HH-CdSe, HH-CdTe, and CT in CdSe/CdTe CQWs. (d) Top: Peak wavelength of CT bleachings at different delay times in dual type-II CQWs. Bottom: The peak wavelength of CT bleachings at different delay times in CdSe/CdTe CQWs. (e) Schematic illustration of the carrier distributions in dual type-II (left) and CdSe/CdTe (right) CQWs.

all the previously reported colloidal nanocrystals. Importantly, transient absorption combined with two-photon excitation spectroscopy has clarified the dominant roles of excited-state absorptions over genuine two-photon absorptions. As a result, the remarkable nonlinear optical performance of dual type-II CQWs is mainly attributed to the ultrafast, efficient, and uniform separation of photoexcited carriers, which boosts the sequential TPA process. These findings not only present a new candidate for optical limiting materials but also enhance the understanding of optical nonlinearity in colloidal nanocrystals.

METHODS

Synthesis of CdSe/CdTe/CdSe CQWs. Core CdSe and CdSe/CdTe CQWs were prepared similarly to our previous report.[31] For the synthesis of CdSe/CdTe/CdSe CQWs, we modified the one-pot synthesis of the multicrowned recipe, which we reported previously.[34] In a typical synthesis, 1 optical density CdSe core CQWs were used as a seed to grow the multicrowned heterostructure. For the core CQWs, a mixture of 0.45 μL of oleic acid, 30 mg of cadmium acetate dihydrate, and 4 mL of octadecene (ODE) was prepared in a flask, which was degassed for 30 min at 100 °C. The inert atmosphere was re-established with the temperature raised to 215 °C. Once the temperature reached, a 0.03 M TOP-Te solution in ODE was introduced at a rate of 15 mL/h with the help of a syringe pump. The solution was kept for 3 min to ensure the depletion of the remaining Te precursors, after injecting the required amount of Te precursor corresponding to the lateral area of the CdTe crown. Once the CdTe layer had grown, the precursor was changed to a 0.03 M TOP-ODE-Se solution, and injection was sustained until the outer CdSe layer reached the desired lateral size. The reaction was annealed for 3 min after the CdSe crown growth reached the target, followed by cooling to room temperature in a water bath. Hexane (3 mL) was injected at 80 °C. Afterward, ethanol was added to wash the products, which were then centrifuged at 6000 rpm for 5 min. The obtained CdSe/CdTe/CdSe CQWs were redissolved and stored in hexane. Please note that the term "core/crown/crown" mainly describes the structure information of CdSe/CdTe/CdSe CQWs, which highlights the formation of two heterointerfaces in these CQWs. While on the other hand, the term "dual type-II" mainly accounts for the band alignment of CdSe/CdTe/CdSe CQWs, which highlights the unique carrier transition/separations process in these CQWs.

https://doi.org/10.1021/acsnano.5c00391
ACS Nano 2025, 19, 9273−9281

Open-Aperture *Z*-Scan Spectroscopy. To investigate the nonlinear optical properties of CdSe/CdTe/CdSe and CdSe/CdTe CQWs at 532 and 800 nm, a homemade *Z*-scan system was utilized. The CQW ensembles were dissolved in hexane to make 0.3 μM solutions and placed in a 1 mm quartz cuvette. For excitation, we used either the second harmonic output from a Q-switched Nd/YAG laser with a 5 ns pulse width or the output from a Ti/sapphire amplifier with a 100 fs pulse width. A 150 mm focal length lens focused the laser pulse onto the sample. The beam waist at $Z = 0$ was measured to be about 12.2 μm using the knife-edge method. A high-precision translation stage held the sample in place, and the transmitted light intensity was measured with a lock-in amplifier (Stanford Research Systems, SR830).

Transient Absorption Spectroscopy. A 1 kHz regenerative amplifier with an 800 nm output wavelength and a 100 fs pulse width, which is seeded by the 80 MHz mode-locked Ti-sapphire oscillators, was used to produce the pump pulse with the maximum energy up to mJ. To generate the white light continuum probe beam spanning from 400 to 1500 nm, we have split a small portion of the fundamental 800 nm pulse from the regenerative amplifier with an energy of ~10 μJ and then incident on sapphire crystals with different thickness for the continuum probe beam generations. A commercial spectrometer was used to collect the probe beam spectra in the ultraviolet−visible region with and without the pump excitations.

ASSOCIATED CONTENT

Supporting Information

The Supporting Information is available free of charge at https://pubs.acs.org/doi/10.1021/acsnano.5c00391.

> TA spectra of dual type-II CQWs under 600 nm excitation; SA behavior of dual type-II CQWs; open aperture *Z*-scan transmission measurements; variation of the normalized transmittance; schematic illustration of the blueshift-redshift crossover; Pseudocolor TA map; wavelength shift of the CT states; comparison of CT PB dynamics (PDF)

AUTHOR INFORMATION

Corresponding Authors

Junhong Yu − *College of Physics and Electronic Engineering, Chongqing Normal University, Chongqing 401331, China; Luminous! Center of Excellence for Semiconductor Lighting and Displays, School of Electrical and Electronic Engineering, School of Physical and Mathematical Sciences, School of Materials Science and Engineering, Nanyang Technological University, 639798, Singapore;* orcid.org/0000-0001-6136-552X; Email: jyu012@e.ntu.edu.sg

Baiquan Liu − *School of Electronics and Information Technology, Sun Yat-Sen University, Guangzhou 510275, China;* orcid.org/0000-0001-9375-7683; Email: liubq33@mail.sysu.edu.cn

Hilmi Volkan Demir − *Luminous! Center of Excellence for Semiconductor Lighting and Displays, School of Electrical and Electronic Engineering, School of Physical and Mathematical Sciences, School of Materials Science and Engineering, Nanyang Technological University, 639798, Singapore; Department of Electrical and Electronics Engineering and Department of Physics, UNAM-Institute of Materials Science and Nanotechnology and the National Nanotechnology Research Center, Bilkent University, Ankara 06800, Turkey;* orcid.org/0000-0003-1793-112X; Email: hvdemir@ntu.edu.sg

Authors

Emek Goksu Durmusoglu − *Luminous! Center of Excellence for Semiconductor Lighting and Displays, School of Electrical and Electronic Engineering, School of Physical and Mathematical Sciences, School of Materials Science and Engineering, Nanyang Technological University, 639798, Singapore;* orcid.org/0000-0001-6840-8342

Yunfei Ren − *School of Electronics and Information Technology, Sun Yat-Sen University, Guangzhou 510275, China*

Wenhui Fang − *School of Electronics and Information Technology, Sun Yat-Sen University, Guangzhou 510275, China*

Yubu Zhou − *School of Electronics and Information Technology, Sun Yat-Sen University, Guangzhou 510275, China*

Linghao Chu − *School of Electronics and Information Technology, Sun Yat-Sen University, Guangzhou 510275, China*

Complete contact information is available at: https://pubs.acs.org/10.1021/acsnano.5c00391

Author Contributions

[#]J.Y. and E.G.D. contributed equally to this work.

Notes

The authors declare no competing financial interest.

ACKNOWLEDGMENTS

This work was supported by the National Key Research and Development Program (2023YFB3611100), the National Natural Science Foundation of China under Grant 12304032; Singapore Agency for Science, Technology and Research (A*STAR) MTC program (Grant No. M21J9b0085). Partial support was also provided by TUBITAK 121C266, and 20AG001. H.V.D. would like to acknowledge the support from the TUBA and TUBITAK 2247-A National Leader Researchers Program.

REFERENCES

(1) Gu, M.; Zhang, Q.; Lamon, S. Nanomaterials for optical data storage. *Nat. Rev. Mater.* **2016**, *1*, No. 16070.

(2) Xu, Y.; Liu, Z.; Zhang, X.; Wang, Y.; Tian, J.; Huang, Y.; Ma, Y.; Zhang, X.; Chen, Y. A Graphene Hybrid Material Covalently Functionalized with Porphyrin: Synthesis and Optical Limiting Property. *Adv. Mater.* **2009**, *21* (12), 1275−1279.

(3) Tutt, L. W.; Boggess, T. F. A review of optical limiting mechanisms and devices using organics, fullerenes, semiconductors and other materials. *Prog. Quantum Electron.* **1993**, *17*, 299−338.

(4) Khan, A. H.; Bertrand, G. H. V.; Teitelboim, A.; Sekhar, M. C.; Polovitsyn, A.; Brescia, R.; Planelles, J.; Climente, J. I.; Oron, D.; Moreels, I. CdSe/CdS/CdTe Core/Barrier/Crown Nanoplatelets: Synthesis, Optoelectronic Properties, and Multiphoton Fluorescence Upconversion. *ACS Nano* **2020**, *14* (4), 4206−4215.

(5) Yu, J.; Dang, C. Colloidal Metal Chalcogenide Quantum Wells for Laser Applications. *Cell Rep. Phys. Sci.* **2021**, *2*, No. 100308.

(6) Xu, Y.; Chen, Q.; Zhang, C.; Wang, R.; Wu, H.; Zhang, X.; Xing, G.; Yu, W. W.; Wang, X.; Zhang, Y.; Xiao, M. Two-Photon Pumped Perovskite Semiconductor Nanocrystal Lasers. *J. Am. Chem. Soc.* **2016**, *138*, 3761−3768.

(7) Wang, F.; Banerjee, D.; Liu, Y.; Chen, X.; Liu, X. Upconversion nanoparticles in biological labeling, imaging, and therapy. *Analyst* **2010**, *135*, 1839−1854.

(8) Chou, K.-L.; Won, N.; Kwag, J.; Kim, S.; Chen, J.-Y. Femto-second laser beam with a low power density achieved a two-photon

photodynamic cancer therapy with quantum dots. *J. Mater. Chem. B* **2013**, *1*, 4584−4592.
(9) Liu, X.; Guo, Q.; Qiu, J. Emerging Low-Dimensional Materials for Nonlinear Optics and Ultrafast Photonics. *Adv. Mater.* **2017**, *29*, No. 1605886.
(10) Calvete, M.; Yang, G. Y.; Hanack, M. Porphyrins and Phthalocyanines as Materials for Optical Limiting. *Synth. Met.* **2004**, *141*, 231−243.
(11) Rath, H.; Sankar, J.; Prabhuraja, V.; Chandrashekar, T. K.; Nag, A.; Goswami, D. Core Modified Expanded Porphyrins with Large Third-Order Nonlinear Optical Response. *J. Am. Chem. Soc.* **2005**, *127*, 11608−11609.
(12) Riggs, J. E.; Walker, D. B.; Carroll, D. L.; Sun, Y. P. Optical limiting properties of suspended and solubilized carbon nanotubes. *J. Phys. Chem. B* **2000**, *104*, 7071−7076.
(13) Yu, X.; Marks, T. J.; Facchetti, A. Metal Oxides for Optoelectronic Applications. *Nat. Mater.* **2016**, *15*, 383−396.
(14) Säynätjoki, A.; Karvonen, L.; Rostami, H.; Autere, A.; Mehravar, S.; Lombardo, A.; Norwood, R. A.; Hasan, T.; Peyghambarian, N.; Lipsanen, H.; Kieu, K.; Ferrari, A. C.; Polini, M.; Sun, Z. Ultra-Strong Nonlinear Optical Processes and Trigonal Warping in MoS_2 Layers. *Nat. Commun.* **2017**, *8*, No. 893.
(15) Li, D.-J.; Li, Q.-H.; Gu, Z.-G.; Zhang, J. Oriented Assembly of 2d Metal-Pyridylporphyrinic Framework Films for Giant Nonlinear Optical Limiting. *Nano Lett.* **2021**, *21* (23), 10012−10018.
(16) Wei, T. C.; Mokkapati, S.; Li, T. Y.; Lin, C. H.; Lin, G. R.; Jagadish, C.; He, J. H. Nonlinear Absorption Applications of $CH_3NH_3PbBr_3$ Perovskite Crystals. *Adv. Funct. Mater.* **2018**, *28*, No. 1707175.
(17) Padilha, L. A.; Nootz, G.; Olszak, P. D.; Webster, S.; Hagan, D. J.; van Stryland, E. W.; Levina, L.; Sukhovatkin, V.; Brzozowski, L.; Sargent, E. H. Optimization of band structure and quantum-size-effect tuning for two-photon absorption enhancement in quantum dots. *Nano Lett.* **2011**, *11*, 1227−1231.
(18) Kagan, C. R.; Lifshitz, E.; Sargent, E. H.; Talapin, D. V. Building devices from colloidal quantum dots. *Science* **2016**, *353*, No. aac5523.
(19) Yu, J.; Sharma, M.; Delikanli, S.; Birowosuto, M. D.; Demir, H. V.; Dang, C. Mutual Energy Transfer in a Binary Colloidal Quantum Well Complex. *J. Phys. Chem. Lett.* **2019**, *10*, 5193−5199.
(20) Kershaw, S. V.; Susha, A. S.; Rogach, A. L. Narrow bandgap colloidal metal chalcogenide quantum dots: synthetic methods, heterostructures, assemblies, electronic and infrared optical properties. *Chem. Soc. Rev.* **2013**, *42*, 3033−3087.
(21) Yu, J.; Hou, S.; Sharma, M.; et al. Strong Plasmon-Wannier Mott Exciton Interaction with High Aspect Ratio Colloidal Quantum Wells. *Matter* **2020**, *2*, 1550−1563.
(22) Burda, C.; Chen, X.; Narayanan, R.; El-Sayed, M. A. Chemistry and Properties of Nanocrystals of Different Shapes. *Chem. Rev.* **2005**, *105*, 1025−1102.
(23) Yu, J.; Sharma, M.; Li, M.; Liu, B.; Hernandez-Martinez, P. L.; Delikanli, S.; Sharma, A.; Altintas, Y.; Hettiarachchi, C.; Sum, T. C.; Demir, H. V.; Dang, C. Efficient generation of emissive many-body correlations in copper-doped colloidal quantum wells. *Cell Rep. Phys. Sci.* **2022**, *3* (9), No. 101049.
(24) Fang, L.-B.; Pan, W.; Zhong, S.-H.; Shen, W.-Z. Nonresonant and Resonant Nonlinear Absorption of CdSe-Based Nanoplatelets. *Chin. Phys. Lett.* **2017**, *34*, No. 098101.
(25) Kalsoom, U. E.; Yi, R. X.; Qu, J. L.; Liu, L. W. Nonlinear Optical Properties of CdSe and CdTe Core-Shell Quantum Dots and Their Applications. *Front. Phys.* **2021**, *9*, No. 612070.
(26) Nyk, M.; Szeremeta, J.; Wawrzynczyk, D.; Samoc, M. Enhancement of Two-Photon Absorption Cross Section in CdSeQuantum Rods. *J. Phys. Chem. C* **2014**, *118*, 17914−17921.
(27) He, G. S.; Yong, K.-T.; Zheng, Q.; Sahoo, Y.; Baev, A.; Ryasnyanskiy, A. I.; Prasad, P. N. Multi-photon excitation properties of CdSe quantum dots solutions and optical limiting behavior in infrared range. *Opt. Express* **2007**, *15* (20), 12818−12833.
(28) Achtstein, A. W.; Ballester, A.; Movilla, J. L.; Hennig, J.; Climente, J. I.; Prudnikau, A.; Antanovich, A.; Scott, R.; Artemyev, M. V.; Planelles, J.; Woggon, U. Linear and two-photon absorption in zero-and one-dimensional CdS nanocrystals: influence of size and shape. *J. Phys. Chem. C* **2015**, *119*, 1260−1267.
(29) Scott, R.; Achtstein, A. W.; Prudnikau, A.; Antanovich, A.; Christodoulou, S.; Moreels, I.; Artemyev, M.; Woggon, U. Two Photon Absorption in II-VI Semiconductors: The Influence of Dimensionality and Size. *Nano Lett.* **2015**, *15* (8), 4985−4992.
(30) Scott, R.; Kickhöfel, S.; Schoeps, O.; Antanovich, A.; Prudnikau, A.; Chuvilin, A.; Woggon, U.; Artemyev, M.; Achtstein, A. W. Temperature dependent radiative and non-radiative recombination dynamics in CdSe-CdTe and CdTe-CdSe type II hetero nanoplatelets. *Phys. Chem. Chem. Phys.* **2016**, *18*, 3197−3203.
(31) Yu, J.; Durmusoglu, E. G.; Wang, Y.; Sharma, M.; Demir, H. V.; Dang, C. Ultrafast Control of the Optical Transition in Type-II Colloidal Quantum Wells. *ACS Photonics* **2023**, *10* (5), 1250−1258.
(32) Pedetti, S.; Ithurria, S.; Heuclin, H.; Patriarche, G.; Dubertret, B. Type-II CdSe/CdTe Core/Crown Semiconductor Nanoplatelets. *J. Am. Chem. Soc.* **2014**, *136* (46), 16430−16438.
(33) Kelestemur, Y.; Olutas, M.; Delikanli, S.; Guzelturk, B.; Akgul, M. Z.; Demir, H. V. Type-II Colloidal Quantum Wells: CdSe/CdTe Core/Crown Heteronanoplatelets. *J. Phys. Chem. C* **2015**, *119* (4), 2177−2185.
(34) Durmusoglu, E. G.; Hu, S.; Hernandez-Martinez, P. L.; Izmir, M.; Shabani, F.; Guo, M.; Gao, H.; Isik, F.; Delikanli, S.; Sharma, V. K.; Liu, B.; Demir, H. V. High External Quantum Efficiency Light-Emitting Diodes Enabled by Advanced Heterostructures of Type-II Nanoplatelets. *ACS Nano* **2023**, *17*, 7636−7644.
(35) Delikanli, S.; Canimkurbey, B.; Hernández-Martínez, P. L.; Shabani, F.; Isik, A. T.; Ozkan, I.; Bozkaya, I.; Bozkaya, T.; Isik, F.; Durmusoglu, E. G.; Izmir, M.; Akgun, H.; Demir, H. V. On the Rational Design of Core/(Multi)-Crown Type-II Heteronanoplatelets. *J. Am. Chem. Soc.* **2023**, *145*, 12033−12043.
(36) Dabard, C.; Guilloux, V.; Gréboval, C.; Po, H.; Makke, L.; Fu, N.; Xu, X. Z.; Silly, M. G.; Patriarche, G.; Lhuillier, E.; Barisien, T.; Climente, J. I.; Diroll, B. T.; Ithurria, S. Double-Crowned 2D Semiconductor Nanoplatelets with Bicolor Power-Tunable Emission. *Nat. Commun.* **2022**, *13* (1), No. 5094.
(37) Diroll, B. T.; Dabard, C.; Hua, M.; Climente, J. I.; Lhuillier, E.; Ithurria, S. Hole Relaxation Bottlenecks in CdSe/CdTe/CdSe Lateral Heterostructures Lead to Bicolor Emission. *Nano Lett.* **2024**, *24*, 7934−7940.
(38) Yu, J.; Demir, H. V.; Sharma, M. Optical signatures of lattice strain in chemically doped colloidal quantum wells. *Nat. Commun.* **2025**, *16*, No. 823.
(39) Li, Q.; Xu, Z.; McBride, J.; Lian, T. Low Threshold Multiexciton Optical Gain in Colloidal CdSe/CdTe Core/Crown Type-II Nanoplatelet Heterostructures. *ACS Nano* **2017**, *11* (3), 2545−2553.
(40) Yu, J.; Sharma, M.; Li, M.; Delikanli, S.; Sharma, A.; Taimoor, M.; Altintas, Y.; McBride, J. R.; Kusserow, T.; Sum, T. C.; Demir, H. V.; Dang, C. Low-Threshold Lasing from Copper-Doped CdSe Colloidal Quantum Wells. *Laser Photonics Rev.* **2021**, *15*, No. 2100034.
(41) Lhuillier, E.; Pedetti, S.; Ithurria, S.; Nadal, B.; Heuclin, H.; Dubertret, B. Two-Dimensional Colloidal Metal Chalcogenides Semiconductors: Synthesis, Spectroscopy, and Applications. *Acc. Chem. Res.* **2015**, *48* (1), 22−30.
(42) Diroll, B. T.; Guzelturk, B.; Po, H.; Dabard, C.; Fu, N.; Makke, L.; Lhuillier, E.; Ithurria, S. 2D II−VI Semiconductor Nanoplatelets: From Material Synthesis to Optoelectronic Integration. *Chem. Rev.* **2023**, *123*, 3543−3624.
(43) Gao, Y.; Li, M.; Delikanli, S.; Zheng, H.; Liu, B.; Dang, C.; Sum, T. C.; Demir, H. V. Low-threshold lasing from colloidal CdSe/CdSeTe core/alloyed-crown type-II heteronanoplatelets. *Nanoscale* **2018**, *10*, 9466−9475.
(44) Vivien, L.; Lancon, P.; Riehl, D.; Hache, F.; Anglaret, E. Carbon Nanotubes for Optical Limiting. *Carbon* **2002**, *40*, 1789−1797.

https://doi.org/10.1021/acsnano.5c00391
ACS Nano 2025, 19, 9273−9281

(45) He, G. S.; Tan, L. S.; Zheng, Q.; Prasad, P. N. Multiphoton absorbing materials: molecular designs, characterizations, and applications. *Chem. Rev.* **2008**, *108* (4), 1245−1330.
(46) Joseph, A.; Elamkulavan, H. J.; Keloth, C.; Aneesh, P. M. Hydrothermally Grown VS_2 Nanosheets: A Material for Optical Limiting Applications. *ACS Appl. Opt. Mater.* **2023**, *1*, 1688−1696.
(47) Gonçalves, I. M.; Medda, A.; Carvalho, A. J. A.; Campos, C. L. A. V.; Ghosh, S.; Gomes, A. S. L.; Patra, A. Nonlinear Optical Properties of 2D CdSe Nanoplatelets in a nonresonant Regime. *J. Phys. Chem. C* **2023**, *127* (33), 16679−16686.
(48) Gao, Y.; Qiu, X.; Zhao, F.; Xiao, S.; Li, J.; Lin, X.; Chen, R.; He, T. Linear and nonlinear photophysical properties of ZnSe/CdS/ZnS core/shell/shell type II nanocrystals. *Photonics Res.* **2020**, *8*, 1416−1421.
(49) Gündoğdu, Y.; Kılıç, H. Ş.; Çadırcı, M. Third order nonlinear optical properties of cdte/cdse quasi type-II colloidal quantum dots. *Opt. Mater.* **2021**, *114*, No. 110956.
(50) Çadirci, M.; Gündoğdu, Y.; Elibol, E.; Kılıç, H. Ş. Nonlinear optical properties of core shell type II quantum dot structures. *Opt. Laser Technol.* **2020**, *128*, No. 106246.
(51) Lu, W.-G.; Chen, C.; Han, D.; Yao, L.; Han, J.; Zhong, H.; Wang, Y. Nonlinear Optical Properties of Colloidal $CH_3NH_3PbBr_3$ and $CsPbBr_3$ Quantum Dots: A Comparison Study Using Z-Scan Technique. *Adv. Opt. Mater.* **2016**, *4* (11), 1732−1737.
(52) Dong, N.; Li, Y.; Feng, Y.; Zhang, S.; Zhang, X.; Chang, C.; Fan, J.; Zhang, L.; Wang, J. Optical Limiting and Theoretical Modelling of Layered Transition Metal Dichalcogenide Nanosheets. *Sci. Rep.* **2015**, *5*, No. 14646.
(53) Wang, Y.; Li, X.; Zhao, X.; Xiao, L.; Zeng, H.; Sun, H. Nonlinear Absorption and Low-Threshold Multiphoton Pumped Stimulated Emission from All-Inorganic Perovskite Nanocrystals. *Nano Lett.* **2016**, *16*, 448−453.
(54) Sun, L.; Zhu, W.; Wang, W.; Yang, F.; Zhang, C.; Wang, S.; Zhang, X.; Li, R.; Dong, H.; Hu, W. Intermolecular Charge-Transfer Interactions Facilitate Two-Photon Absorption in Styrylpyridine-Tetracyanobenzene Cocrystals. *Angew. Chem., Int. Ed.* **2017**, *56*, 7831−7835.
(55) Pandya, R.; Chen, R. Y. S.; Cheminal, A.; Dufour, M.; Richter, J. M.; Thomas, T. H.; Ahmed, S.; Sadhanala, A.; Booker, E. P.; Divitini, G.; Deschler, F.; Greenham, N. C.; Ithurria, S.; Rao, A. Exciton-Phonon Interactions Govern Charge-Transfer-State Dynamics in CdSe/CdTe Two-Dimensional Colloidal Heterostructures. *J. Am. Chem. Soc.* **2018**, *140*, 14097−14111.
(56) He, J.; Qu, Y.; Li, H.; Mi, J.; Ji, W. Three-photon absorption in ZnO and ZnS crystals. *Opt. Express* **2005**, *13*, 9235−9247.
(57) Li, Q.; Zhou, B.; McBride, J.; Lian, T. Efficient Diffusive Transport of Hot and Cold Excitons in Colloidal Type II CdSe/CdTe Core/Crown Nanoplatelet Heterostructures. *ACS Energy Lett.* **2017**, *2* (1), 174−181.
(58) Yu, J.; Sharma, M.; Wang, Y.; Delikanli, S.; Baruj, H. D.; Sharma, A.; Demir, H. V.; Dang, C. Modulating Emission Properties in a Host-Guest Colloidal Quantum Well Superlattice. *Adv. Opt. Mater.* **2022**, *10*, No. 2101756.

https://doi.org/10.1021/acsnano.5c00391
ACS Nano 2025, 19, 9273−9281